Available online at www.sciencedirect.com
SCIENCE DIRECT®
PERGAMON
International Journal of Heat and Mass Transfer 46 (2003) 4013–4021
International Journal of HEAT and MASS TRANSFER
www.elsevier.com/locate/ijhmt

Solidification of a supercooled liquid in stagnation-point flow

R.A. Lambert, R.H. Rangel *

Department of Mechanical and Aerospace Engineering, University of California, Irvine, CA 92697-3975, USA

Received 25 October 2002; received in revised form 28 April 2003

Abstract

The solidification of a thermally supercooled liquid in stagnation-point flow is investigated. Due to the advancing solidifying front, both the temperature and flow fields are time dependent. A numerical solution to the problem using an interface tracking method is compared to analytical solutions obtained for instantaneous similarity (short time solution) and quasi-steady state (long time solution). The results show that the velocity of the solid–liquid interface eventually reaches a constant value and that the magnitude of the interface velocity increases with greater thermal supercooling. The solution to this problem provides insight into more complicated solidification problems relating to crystal growth.

1. Introduction

The behavior of the transient temperature field and the solidification process is investigated for a supercooled liquid in the presence of forced convective flow. The convective flow evaluated in this analysis is stagnation-point flow, which can be observed under such conditions as a liquid poured into a mould, directional solidification of a multi-component material at the onset of thermosolutal convection, or buoyancy driven flows [1–3]. Stagnation-point flow solidification has been investigated for homogeneous and multi-component materials [1,2,4–6]; however the behavior of the solidification process is sensitive to the boundary conditions. Due to the non-linearity of the boundary conditions [7], analytical solutions to the governing equations are limited and have been used in phase-change problems in a semi-infinite domain without convection [8,9]. In this study approximate analytical and numerical methods are used to solve solidification in a semi-infinite domain with convection, which can be used as a basis in complex solidification problems such as crystal growth.

The numerical methods for solving the phase change problem with moving boundaries have been categorized into two types: the enthalpy method which treats the enthalpy as a variable, and transformation methods in which the position of the interface is tracked using the heat balance equation at the solid–liquid interface [10–12]. The enthalpy method has been shown to be more accurate for materials with a range in phase-change temperatures such as alloys. For a material with one phase change temperature the enthalpy method has been shown to contain inaccuracies near the phase-change boundary [12]. Experiments and theoretical investigations of stagnation-point flow solidification in a semi-infinite domain for a warm liquid in contact with a solid layer have been conducted [4–6]. During solidification under forced convection of this type, it has been demonstrated that the thickness of the solid region reaches a constant value. This finding was also observed in convective flow of warm water parallel to a frozen layer [13].

The governing equations in this analysis are solved using the analytical and numerical methods applied by Bian and Rangel [5,6] to a similarly posed problem. In the present problem, the solution methods provide insight into the solidification of a thermally supercooled liquid. In the mathematical formulation of this problem, solidification occurs within a semi-infinite domain and it is assumed that the material is homogeneous with constant density in the solid and liquid phases. Analytical solutions to the governing equations are available in the

* Corresponding author. Tel.: +1-949-824-4033; fax: +1-949-824-8585.
E-mail address: rhrangel@uci.edu (R.H. Rangel).

0017-9310/03/$ - see front matter © 2003 Elsevier Ltd. All rights reserved.
doi:10.1016/S0017-9310(03)00248-5

Nomenclature

A	potential flow strain, s^{-1}
c_p	specific heat, J/kg K
h_{sf}	specific latent heat of fusion, J/kg
s	thickness of the solid phase, m
$\dot{s}$	dimensionless solid–liquid interface velocity, $d\tilde{s}/d\tau$
$\tilde{s}$	dimensionless solid phase thickness, $s\sqrt{A/\alpha_l}$
Ste	Stefan number, $\mathrm{Ste} = c_p(T_m - T_i)/h_{sf}$
T	temperature, K
t	time, s
u	fluid velocity normal to the solid–liquid interface, m/s
v	fluid velocity tangent to the solid–liquid interface, m/s
x	spatial coordinate normal to the solid–liquid interface, m
$\tilde{x}$	dimensionless spatial coordinate, $x\sqrt{A/\alpha_l}$
x'	transformed spatial coordinate in the finite domain, $2/\pi \tan^{-1}(x/s)$
y	spatial coordinate tangent to the solid–liquid interface, m

Greek symbols

α	thermal diffusivity, m^2/s
β	parameter used in numerical analysis
κ	thermal conductivity, W/mK
θ	dimensionless temperature, $(T - T_i)/(T_m - T_i)$
λ	solidification parameter, similarity solutions
λ^*	solidification parameter, long time solution
η	similarity variable
ρ	density, kg/m^3
ξ	transformed spatial coordinate normal to the interface, $\xi = x - s(t)$, m
$\tilde{\xi}$	dimensionless spatial coordinate, $\tilde{\xi} = \xi\sqrt{A/\alpha_l}$
τ	dimensionless time, At

Subscripts

i	far field
l	liquid phase
m	solid–liquid equilibrium
s	solid phase

small time and quasi-steady state regimes. The numerical method used in this analysis is an interface tracking method in a transformed coordinate system.

2. Problem description

During solidification of a supercooled liquid in a half-space, the initial temperature of the liquid, T_i, is below the melting temperature of the homogeneous material, T_m, as shown in Fig. 1. The solid phase is maintained at the equilibrium solidification temperature. In the liquid region, the flow field is decoupled from the thermal field by assuming constant density and no viscous dissipation. However, since the solidification front is moving with respect to time, the thermal field and the flow field are not fully independent of one another.

For materials such as metals, the Prandtl number is very small resulting in a thermal boundary layer that is much larger than the viscous boundary layer. For stagnation-point flow of a material with a very small Prandtl number, the viscous effects are negligible and the potential flow field approximation maybe used. The quasi-steady solution of the inviscid two-dimensional stagnation flow field becomes,

$$u = -2A(x - s(t)), \tag{1}$$

in the x direction (normal to the interface), and

$$v = 2Ay, \tag{2}$$

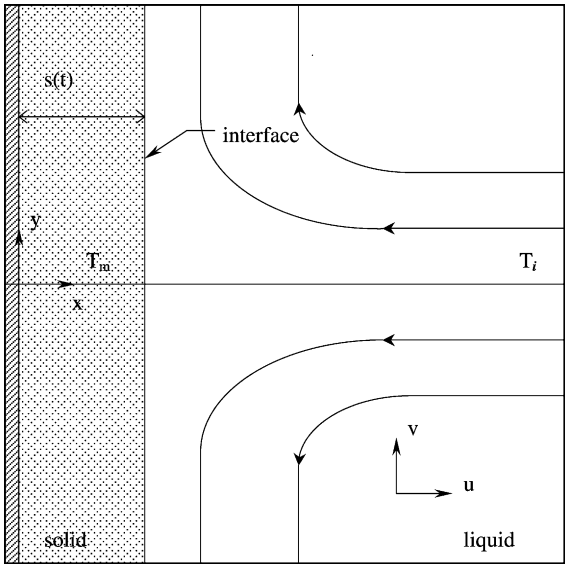

Fig. 1. Stagnation-point flow solidification of a supercooled liquid in a half-space.

in the y direction parallel to the interface. The potential flow field is shown in Fig. 1.

Because the temperature in the solid phase is maintained constant, the governing equation is the two-dimensional energy equation in the liquid phase,

$$\frac{\partial T_l}{\partial t} + u\frac{\partial T_l}{\partial x} + v\frac{\partial T_l}{\partial y} = \alpha_l\left(\frac{\partial^2 T_l}{\partial x^2} + \frac{\partial^2 T_l}{\partial y^2}\right). \quad (3)$$

When the solidifying front is planar, heat transfer occurs in one direction and Eq. (3) reduces to the one dimensional transport equation,

$$\frac{\partial T_l}{\partial t} + u\frac{\partial T_l}{\partial x} = \alpha_l\frac{\partial^2 T_l}{\partial x^2}. \quad (4)$$

The velocity and position of the advancing interface is found by solving the heat balance equation at the liquid–solid interface,

$$\rho h_{sf}\frac{ds}{dt} = -\kappa_l\frac{\partial T_l}{\partial x}\bigg|_{x=s(t)}. \quad (5)$$

It is evident from the flow field equations (1) and (2) that the velocity normal to the interface is a function of the position of the moving interface. The changing boundary condition at the interface leads to a temperature field that is dependent upon the flow field. Numerical methods are used to solve Eq. (4). The behavior of the thermal field is investigated analytically by looking at the long time behavior and an instantaneous similarity solution as time approaches zero.

3. Long time solution

The stagnation-point flow transports the liquid with an initial far field temperature, T_i, toward the solidifying front, which is at the melting temperature of the material. After a long time, the temperature gradient in the liquid is expected to reach a constant value. In the absence of stagnation-point flow, Carslaw and Jaeger [8] show that the velocity of the advancing solid–liquid interface is proportional to $t^{-1/2}$. In this problem, with the addition of stagnation-point flow, the velocity of the solidifying front, ds/dt, is expected to be a constant independent of time as the thermal field approaches steady state.

The long time solution is found by assuming that the system has reached quasi-steady state. The interface velocity is determined using Eq. (5), the heat balance equation at the solid–liquid interface. The one dimensional energy transport equation,

$$\frac{\partial T_l}{\partial t} - 2A(x - s(t))\frac{\partial T_l}{\partial x} = \alpha_l\frac{\partial^2 T_l}{\partial x^2}, \quad (6)$$

is transformed to a coordinate system moving with the solid–liquid interface,

$$A\frac{\partial T_l}{\partial \tau} - \left(A\frac{ds}{d\tau} + 2A\xi\right)\frac{\partial T_l}{\partial \xi} = \alpha_l\frac{\partial^2 T_l}{\partial \xi^2}. \quad (7)$$

In dimensionless form, the steady state equation becomes,

$$\frac{\partial^2 T_l}{\partial \tilde{\xi}^2} + \left(\frac{d\tilde{s}}{d\tau} + 2\tilde{\xi}\right)\frac{\partial T_l}{\partial \tilde{\xi}} = 0. \quad (8)$$

Eq. (8) is solved using boundary conditions in the far field and at the solid–liquid interface. The boundary conditions are $T_l = T_i$ as x approaches infinity, and $T_l = T_m$ at the interface $x = s(t)$. The liquid temperature profile of the long time solution is,

$$\theta_l = \frac{T_l - T_i}{T_m - T_i} = \frac{\operatorname{erfc}\left(\tilde{\xi} + \frac{\dot{s}}{2}\right)}{\operatorname{erfc}\frac{\dot{s}}{2}}. \quad (9)$$

The condition at the solid–liquid interface, Eq. (5), is expressed in dimensionless form,

$$\dot{s} = -\mathrm{Ste}\frac{\partial \theta_l}{\partial \tilde{\xi}}\bigg|_{\tilde{\xi}=0}, \quad (10)$$

where the Stefan number, Ste, is a measure of the amount of thermal supercooling in the liquid phase.

Combining Eqs. (9) and (10), the velocity of the solid–liquid interface is expressed as,

$$\dot{s}\exp\left(\frac{\dot{s}}{2}\right)^2\operatorname{erfc}\frac{\dot{s}}{2} = \frac{2}{\sqrt{\pi}}\mathrm{Ste}. \quad (11)$$

Eq. (11) confirms the initial assumption that, after a long time, the velocity of the solidifying front is constant. Therefore, the relationship between the thickness of the solidifying front, $\tilde{s}$, and time is linear and can be expressed in terms of a constant,

$$\tilde{s}(\tau) = 2\lambda^*\tau, \quad (12)$$

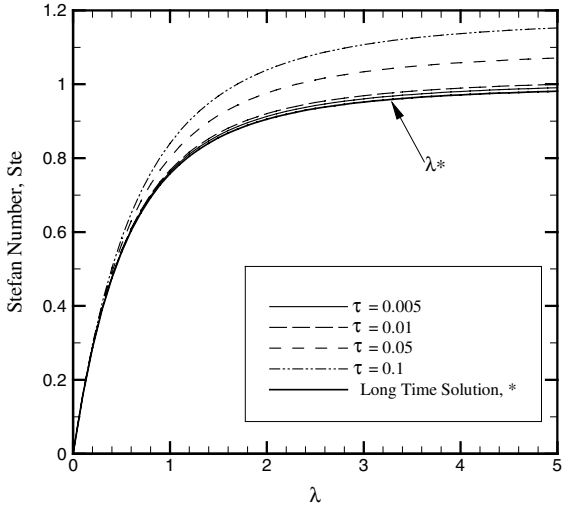

Fig. 2. Relationship between the Stefan number and the solidification parameter derived from the heat balance equation at the solid–liquid interface for the instantaneous similarity solution and the long time solution.

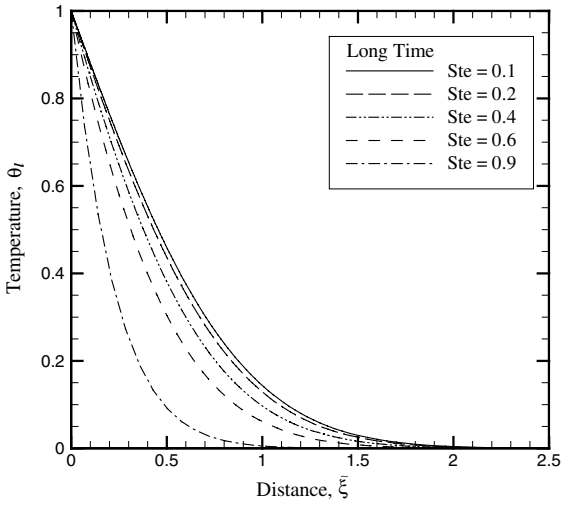

Fig. 3. Long time solution of the temperature profile in stagnation-point flow solidification for values of the Stefan number.

where $\lambda^* = \tilde{s}(\tau)/2\tau$ is a solidification parameter for the long time solution with a factor of 2 introduced for convenience. In Eq. (11) the speed of the moving front depends upon the amount of thermal supercooling in the fluid, as indicated by the Stefan number. A graph of the parameter λ^* versus the Stefan number is shown in Fig. 2. The figure shows that as the Stefan number approaches 1, the terminal velocity of the solid–liquid interface approaches infinity. The Stefan number is thus limited to values less than 1.0. Beyond this value, no solution can be found for Eq. (11) which indicates that the liquid could not be maintained in such high level of supercooling and would freeze instantaneously.

The quasi-steady temperature profile in the liquid phase, derived from the long time solution is shown in Fig. 3 for different values of the Stefan number. Fig. 3 shows that the temperature gradient increases as the amount of thermal supercooling in the liquid region increases.

4. Instantaneous similarity solution

Instantaneous similarity is analogous to the concept of local similarity in a flow field, where a solution is independent of the position along a streamline and is "locally autonomous". Using a similarity variable, the partial differential equation (4) is transformed into an ordinary differential equation in a new coordinate system. Bian and Rangel [6] have applied the concept of instantaneous similarity in stagnation-point flow solidification to find solutions at very small times. During our earlier derivation of the long time solution, the coordinate system was placed at the moving solid–liquid interface. For instantaneous similarity, the coordinate system remains at the wall. The similarity variable used in this analysis is,

$$\eta = \frac{\tilde{x}}{2\sqrt{\tau}}, \tag{13}$$

and we define a solidification parameter based on the non-convective solution [8] as,

$$\lambda = \frac{\tilde{s}}{2\sqrt{\tau}}. \tag{14}$$

The energy equation (4) expressed in terms of the new variables is,

$$\tau\frac{\partial T_l}{\partial \tau} - \left(\frac{\eta}{2} + 2\tau(\eta - \lambda)\right)\frac{\partial T_l}{\partial \eta} = \frac{1}{4}\frac{\partial^2 T_l}{\partial \eta^2}. \tag{15}$$

In instantaneous similarity, the derivatives with respect to time are set to zero and Eq. (15) becomes,

$$\frac{1}{4}\frac{\partial^2 T_l}{\partial \eta^2} + \left(\frac{\eta}{2} + 2\tau(\eta - \lambda)\right)\frac{\partial T_l}{\partial \eta} = 0. \tag{16}$$

The liquid phase temperature is derived using the following boundary conditions: $T_l = T_m$ at the solid–liquid interface and $T_l = T_i$ as η approaches infinity. From the solution in Eq. (16), the temperature profile in the liquid phase is expressed as,

$$\theta_l = \operatorname{erfc}\left(\frac{4\tau(\eta - \lambda) + \eta}{\sqrt{4\tau + 1}}\right) \Big/ \operatorname{erfc}\left(\frac{\lambda}{\sqrt{4\tau + 1}}\right). \tag{17}$$

The condition at the solid–liquid interface, Eq. (5), expressed in terms of the new coordinate system is,

$$\frac{d\tilde{s}}{d\tau} = -\frac{\mathrm{Ste}}{2\sqrt{\tau}}\frac{\partial \theta_l}{\partial \eta}. \tag{18}$$

Combining Eqs. (17) and (18), the solidification parameter is expressed as a function of time,

$$\lambda \exp\left(\frac{\lambda}{\sqrt{4\tau + 1}}\right)^2 \operatorname{erfc}\left(\frac{\lambda}{\sqrt{4\tau + 1}}\right) = \frac{\mathrm{Ste}}{\sqrt{\pi}}. \tag{19}$$

When $\tau = 0$, Eq. (19) reduces to the classic equation [8] for solidification of a supercooled liquid in the absence of convection. This finding is similar to the instantaneous similarity results of Bian and Rangel [6], for a stagnation-flow solidification problem of a superheated liquid. Fig. 2 shows the relationship between the Stefan number and values of the solidification parameter, λ, for values of τ ranging from 0.005 to 0.1. Similarly, as the solidification parameter increases, the Stefan number approaches a maximum value above 1, which is only valid for a range in small time values. As the value of τ increases, the maximum Stefan number increases until the instantaneous similarity solution no longer describes the behavior of the temperature profile. A range of values for the solidification parameter, λ, the

Table 1
Conditions at the solid–liquid interface for the instantaneous similarity solution

τ	Stefan number	λ	$\dot{s}$	$\tilde{s}(\tau)$
0.005	0.1	0.060	0.853	0.009
	0.2	0.130	1.83	0.018
	0.4	0.309	4.37	0.044
	0.6	0.588	8.31	0.083
	0.9	1.845	26.1	0.261
0.01	0.1	0.060	0.602	0.012
	0.2	0.130	1.30	0.026
	0.4	0.308	3.08	0.062
	0.6	0.583	5.83	0.117
	0.9	1.770	17.7	0.354
0.05	0.1	0.060	0.27	0.027
	0.2	0.128	0.57	0.057
	0.4	0.300	1.34	0.134
	0.6	0.551	2.47	0.247
	0.9	1.409	6.30	0.630

interface velocity, $\dot{s}$, and the thickness of the solid region, $\tilde{s}(\tau)$, are listed in Table 1. As τ increases, the interface velocity and thickness increase, while the value of the solidification parameter decreases. For increasing values of the Stefan number, the values of these interface parameters increase for any value of time, τ.

The temperature profile at $\tau = 0.005$ for different values of the Stefan number is illustrated in Fig. 4. The figure shows that as the Stefan number increases the temperature gradient in the liquid phase increases.

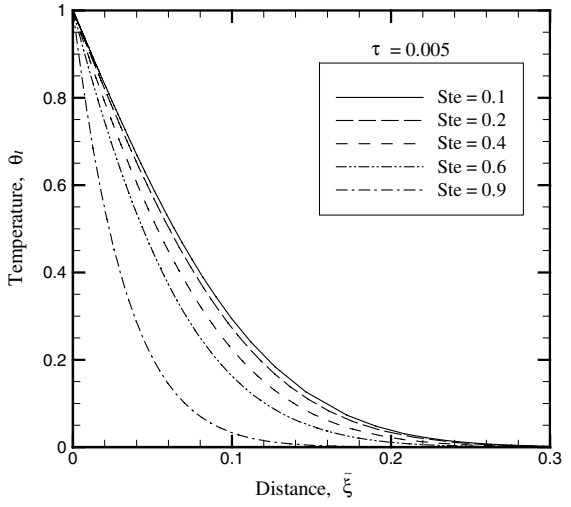

Fig. 4. Temperature profile of the instantaneous solution in the liquid phase when $\tau = 0.005$. The temperature is plotted over a range of Stefan numbers that is less than the maximum Stefan number.

5. Numerical solution

Analytical methods were used above to solve the energy equation for the quasi-steady state and short time solutions. For the unsteady temperature profile in the liquid phase, the numerical methods used by Bian and Rangel [5] to solve stagnation flow solidification in a half space are used to solve the transport equation (4). To solve the full transport equation in a semi-infinite domain, Bian and Rangel transformed the coordinate system into a finite domain using a trigonometric transformation. In order to resolve the moving boundary, the position of the solid–liquid interface is derived from the heat balance equation (5), at the solid–liquid interface. The results of the numerical analysis are compared with the instantaneous similarity and long-term solutions.

In the analysis, solidification takes place in a semi-infinite domain. The governing equations (4) and (5), are transformed into a new coordinate system (x', τ), such that the semi-infinite domain becomes bounded between $0.5 \leqslant x' \leqslant 1$ with $x' = 0.5$ at the solid–liquid interface. For a fixed value of x', the coordinate in the semi-infinite domain, x, moves farther away from the solid–liquid interface as s increases. The relationship between x' and x shows that while the coordinate system remains fixed in the numerical analysis, the values derived for the temperature field are moving farther from the interface in the semi-infinite domain as time increases.

The transformations are as follows:

$$\frac{\partial}{\partial t} = A\frac{\partial}{\partial \tau} - \frac{A}{\pi}\sin(\pi x')\frac{1}{\tilde{s}}\frac{\mathrm{d}\tilde{s}}{\mathrm{d}\tau}\frac{\partial}{\partial x'}, \tag{20}$$

$$\frac{\partial}{\partial x} = \frac{2}{\pi}\sqrt{\frac{A}{\alpha_l}}\cos^2\left(\frac{\pi}{2}x'\right)\frac{1}{\tilde{s}}\frac{\partial}{\partial x'}, \tag{21}$$

and

$$\frac{\partial^2}{\partial x^2} = -\frac{2A}{\pi\alpha_l}\sin(\pi x')\cos^2\left(\frac{\pi}{2}x'\right)\frac{1}{\tilde{s}^2}\frac{\partial}{\partial x'} + \frac{4A}{\pi^2\alpha_l}\cos^4\left(\frac{\pi}{2}x'\right)\frac{1}{\tilde{s}^2}\frac{\partial^2}{\partial x'^2}. \tag{22}$$

Substituting Eqs. (20)–(22) into Eqs. (4) and (5), the energy transport and the heat balance equations are expressed as,

$$\frac{\partial\theta_l}{\partial\tau} = \frac{4}{\pi^2}\cos^4\left(\frac{\pi}{2}x'\right)\frac{1}{\tilde{s}^2}\frac{\partial^2\theta_l}{\partial x'^2} + \left(\frac{1}{\pi}\sin(\pi x')\frac{\dot{s}}{\tilde{s}} + \frac{2}{\pi}\sin(\pi x') - \frac{4}{\pi}\cos^2\left(\frac{\pi}{2}x'\right) - \frac{2}{\pi}\sin(\pi x')\cos^2\left(\frac{\pi}{2}x'\right)\frac{1}{\tilde{s}^2}\right)\frac{\partial\theta_l}{\partial x'} \tag{23}$$

and

$$-\frac{\pi\tilde{s}}{\mathrm{Ste}}\dot{s} = \left.\frac{\partial\theta_1}{\partial x'}\right|_{x'=0.5} \tag{24}$$

for $0.5 \leqslant x' \leqslant 1$.

The energy transport equation (23) is transformed into algebraic form using the Crank–Nicolson scheme [14]. Expressed in finite-difference form, Eq. (23) becomes,

$$\frac{\theta_j^{n+1}-\theta_j^n}{\Delta\tau} = \frac{A}{2}\left(\frac{\theta_{j+1}^{n+1}-2\theta_j^{n+1}+\theta_{j-1}^{n+1}}{\Delta x'^2}+\frac{\theta_{j+1}^{n}-2\theta_j^{n}+\theta_{j-1}^{n}}{\Delta x'^2}\right) + \frac{B}{2}\left(\frac{\theta_{j+1}^{n+1}-\theta_{j-1}^{n+1}}{2\Delta x'}+\frac{\theta_{j+1}^{n}-\theta_{j-1}^{n}}{2\Delta x'}\right), \tag{25}$$

where

$$\beta = \tilde{s}^2, \tag{26}$$

$$A = \frac{4}{\pi^2}\cos^4\left(\frac{\pi}{2}x'_j\right)\frac{1}{\beta^{n+1}}, \tag{27}$$

$$B = \frac{1}{2\pi}\sin(\pi x'_j)\frac{1}{\beta^{n+1}}\frac{\mathrm{d}\beta^{n+1}}{\mathrm{d}\tau} + \frac{2}{\pi}\sin(\pi x'_j) - \frac{4}{\pi}\cos^2\left(\frac{\pi}{2}x'_j\right) - \frac{2}{\pi}\sin(\pi x'_j)\cos^2\left(\frac{\pi}{2}x'_j\right)\frac{1}{\beta^{n+1}}. \tag{28}$$

The superscript n refers the number of time iterations while the subscript j refers to the position along the finite difference grid in the x' direction. Eq. (25) is rewritten as,

$$-(d_1+d_2)\theta_{j-1}^{n+1}+(1+2d_1)\theta_j^{n+1}-(d_1-d_2)\theta_{j-1}^{n+1} = (d_1+d_2)\theta_{j-1}^{n}+(1-2d_1)\theta_j^{n}+(d_1-d_2)\theta_{j-1}^{n}, \tag{29}$$

where

$$d_1 = \frac{A\Delta\tau}{2\Delta x'^2}, \tag{30}$$

and

$$d_2 = \frac{B\Delta\tau}{4\Delta x'}. \tag{31}$$

The Thomas algorithm [15] is used to solve the tridiagonal matrix in Eq. (29) for the following boundary conditions,

$$\theta_1 = 1 \quad \text{at } x' = 0.5 \tag{32}$$

and

$$\theta_1 = 0 \quad \text{at } x' = 1.0. \tag{33}$$

The heat balance equation at the liquid–solid interface, Eq. (24), is transformed into a semi-discrete form with a time derivative on the left and the algebraic flux terms on the right. The ordinary differential equation is,

$$f^n = \left(\frac{\mathrm{d}\beta}{\mathrm{d}\tau}\right)^n = -\frac{2\mathrm{Ste}}{\pi}\frac{(-\theta_3^n+4\theta_2^n-3\theta_1^n)}{2\Delta x'}, \tag{34}$$

where f, is the flux term. The flux is only calculated at the solid–liquid interface using the temperature values at first three nodes of the finite difference grid. An improved Euler scheme is used to solve for the conditions at the interface, such as the variable position of the solid–liquid interface, β, and the interface velocity, $\dot{s}$, and is expressed as,

$$\beta^* = \beta^n + \Delta\tau f^n. \tag{35}$$

The value of β^* is used in Eq. (29) to obtain a new value for the flux, f^* in Eq. (34). The value for β at the new time step, $n+1$, is,

$$\beta^{n+1} = \beta^n + 0.5\Delta\tau(f^* + f^n). \tag{36}$$

The process of using Eqs. (34) and (35) to determine the values of the flux, f, and the parameter, β, at the new time step is repeated until the change in the values of the time varying solutions are less than a tolerance error, $\varepsilon = 10^{-4}$. In the numerical analysis it was observed that decreasing the tolerance level did not result in significant changes in the final numerical predictions and only increased the process time. The accuracy of the numerical solution is determined by comparing the numerical predictions of the quasi-steady state interface velocity with the value from the long time solution in Eq. (11). Initially, grid spacing of $\Delta x' = 0.01$ and a time step of $\Delta\tau = 10^{-4}$ were used, however, for Stefan numbers greater than 0.1, values of the grid spacing, $\Delta x' = 0.0025$, and the time step, $\Delta\tau = 10^{-5}$, resulted in improved convergence of the numerical solution. For smaller grid spacing and time step values, the numerical accuracy of the solution did not improve and the solution had a tendency to diverge.

6. Results

At $\tau = 0$, the parameter, β, is zero leading to a singularity in Eq. (25) at the first time step. Bian and Rangel [5] avoid the singularity by beginning the numerical analysis at a small time $\tau = \tau_0$, with an initial temperature profile calculated from the instantaneous similarity solution. In this analysis, Eqs. (14), (17), and (19) derived in the instantaneous similarity solution, are used to calculate the position of the interface, $\tilde{s}$, and the initial temperature profile at a small initial time value, τ_0. The initial temperature profiles and the numerical solution of Eq. (23) are shown in Fig. 5 for a Stefan number of 0.4 (Fig. 5a), and for a Stefan number of 0.9 (Fig. 5b). Fig. 5a and b show the numerical solution at $\tau = 1.0$ using three different values of the starting time, $\tau_0 = 0.005$, 0.01, and 0.05, used for the initial tempera-

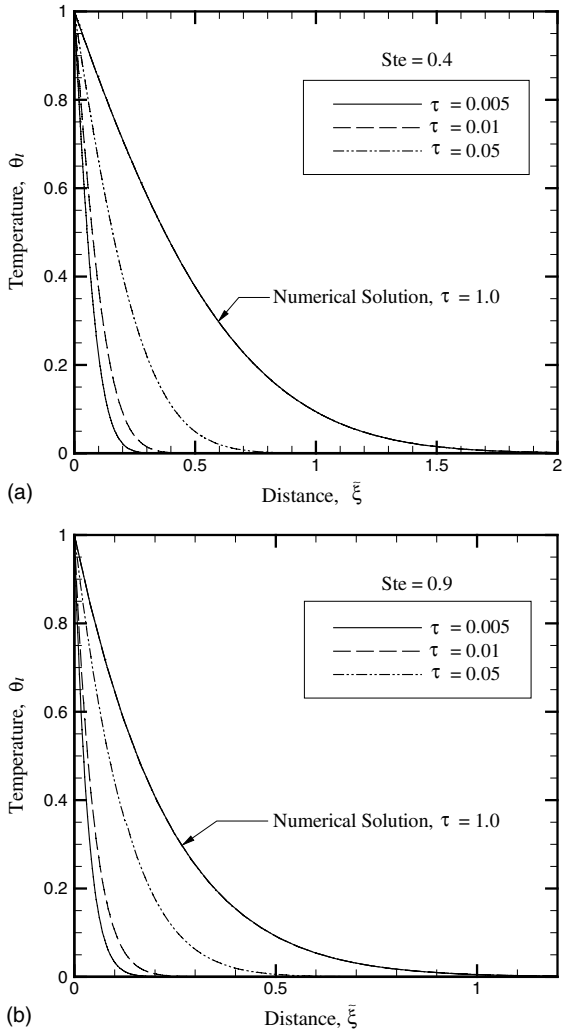

Fig. 5. Comparison between the numerical solution of the temperature field at $\tau = 1.0$ and the initial liquid temperature profile calculated using the instantaneous similarity solution for initial time values ranging from 0.005 to 0.05 for (a) a Stefan number of 0.4 and (b) a Stefan number of 0.9.

ture profile in the instantaneous similarity equations. The graphs show that the numerical results are not sensitive to the initial time value as long as the instantaneous similarity assumption remains valid, confirming an observation made by Bian and Rangel [5]. The graphs also illustrate that this observation does not change with the Stefan number. Since the numerical solution is not sensitive to the initial time value, a value of $\tau_0 = 0.01$ is used in the numerical analysis. Fig. 5 shows that this value of τ_0 is sufficiently small and has no relevant impact on the numerical solution.

The numerical calculations of the velocity of the solid–liquid interface, $\dot{s}$, versus time is shown in Fig. 6

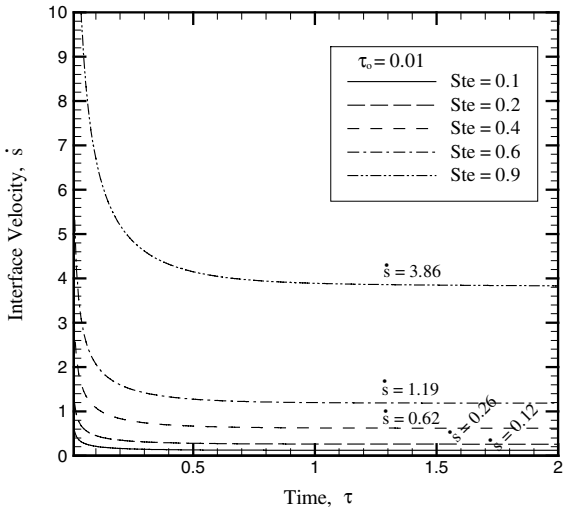

Fig. 6. Numerical calculation of the solid–liquid interface velocity versus time for values of the Stefan number. After a long time, the interface velocity approaches a constant value.

for different values of the Stefan number. The interface velocity decreases in time until a constant velocity is reached. For increases in the Stefan number, the velocity of the solid–liquid interface increases at any given time. This result illustrates that the solidification process is faster for increases in thermal supercooling. When the time value is 2, Fig. 6 illustrates that steady state in the liquid region, or constant interface velocity, has been reached for the range of solidification parameters shown in the graph. The numerical calculation of the constant interface velocity is compared to the value calculated from the long time solution in Eq. (11) in Table 2 and in Fig. 6 at $\tau = 2$. The difference between the interface velocity calculated using the numerical solution and Eq. (11) ranges from 0.08% to 4% with increasing numerical error for higher values of the Stefan number.

Fig. 7 shows the unsteady temperature profiles derived in the numerical analysis for a Stefan number of 0.4 (Fig. 7a) and 0.8 (Fig. 7b). As the Stefan number increases, the temperature gradient in the liquid phase increases, following the trends observed in the previous analytical analyses (quasi-steady and instantaneous similarity solutions). The temperature profiles derived from the numerical analysis are given for $\tau = 0.1$, 0.2, 0.4, 0.6, and 0.8. The temperature profiles for the instantaneous similarity solution at $\tau = 0.01$ and the long time solution at $\tau = 1.0$, are included in the figures. The results from the numerical analysis show that as time increases, the unsteady temperature profile approaches the quasi-steady state solution expressed in Eq. (9) for a moving frame of reference, $\tilde{\xi}$. The time for the temperature field to reach quasi-steady state, increases slightly as the Stefan number increases.

Table 2
Conditions at the solid–liquid interface after a long time

Stefan number	Long time solution		Numerical solution	% Error, $\dot{s}$
	λ^*	$\dot{s}$, Eq. (11)	$\dot{s}$	
0.1	0.060	0.121	0.121	0.08%
0.2	0.130	0.260	0.260	0.00%
0.4	0.310	0.620	0.620	0.03%
0.6	0.593	1.186	1.187	0.1%
0.9	1.930	3.860	3.706	4.0%

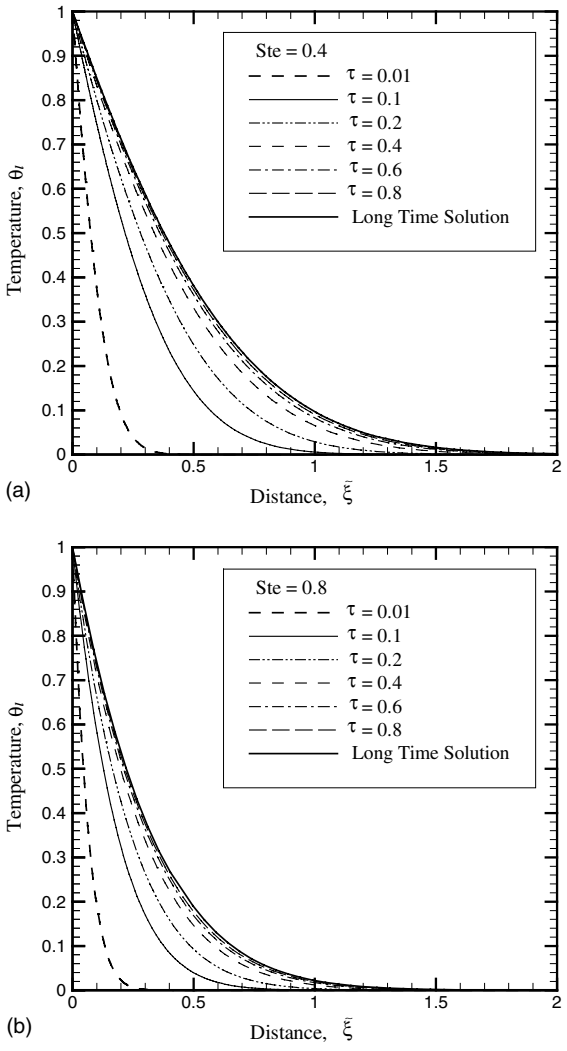

Fig. 7. Numerical solution of the temperature profile in the liquid phase for (a) Ste = 0.4 and (b) Ste = 0.8. The numerical solution converges to the long time solution.

7. Conclusion

Stagnation-point flow solidification of a supercooled liquid in a half space was solved using analytical and numerical methods. The viscous effects for a material with a high Prandtl number are negligible, allowing the potential flow field assumption. An evaluation of the long time solution, or quasi-steady state solution, of the energy equation showed that the interface velocity reaches a constant value after an initial time period and that the magnitude of the velocity increases with increasing thermal supercooling. From the heat balance equation at the solid–liquid interface, the analysis shows that a limit on the amount of thermal supercooling in the liquid phase exists, with a maximum Stefan number approaching a value of 1 at quasi-steady state. The amount of thermal supercooling in the liquid governs the magnitude of the final velocity of the solid–liquid interface. For both the long time and instantaneous solutions of the energy equation, the gradient of the temperature profile in the liquid phase increases as the Stefan number increases.

Numerical methods were used to solve for the unsteady temperature profile. The results from the numerical analysis show that the temperature profile in the liquid phase reaches quasi-steady state, or the long time solution, after an initial time period. The time for the temperature field to reach quasi-steady state increases slightly with increasing values of the Stefan number. The velocity of the solid–liquid interface is observed to decrease in time until a constant value predicted by the long time solution, is reached.

References

[1] K. Brattkus, S.H. Davis, Flow induced morphological instabilities: stagnation-point flows, J. Cryst. Growth 89 (1988) 423–427.
[2] R.A. Brown, D.H. Kim, Modeling of directional solidification: from Scheil to detailed numerical simulation, J. Cryst. Growth 109 (1991) 50–65.
[3] L. Buhler, S.H. Davis, Flow-induced changes of the morphological stability in directional solidification: localized morphologies, J. Cryst. Growth 186 (1998) 629–647.
[4] J.M. Savino, J.F. Zumdieck, R. Siegel, Experimental study of freezing and melting of flowing warm water at a stagnation point on a cold plate, in: U. Grigull, E. Hahne (Eds.), Fourth International Heat Transfer Conference

Versailles, September 1970, Elsevier, Amsterdam, 1970–1971.
[5] X. Bian, R.H. Rangel, Numerical solution of the inviscid stagnation-flow solidification problem, Numer. Heat Transfer, Part A 28 (1995) 589–603.
[6] X. Bian, R.H. Rangel, The inviscid stagnation-flow solidification problem, Int. J. Heat Mass Transfer 39 (1996) 1591–1602.
[7] M. Epstein, F.B. Cheung, Complex freezing-melting interfaces in fluid flow, Annu. Rev. Fluid Mech. 15 (1983) 293–319.
[8] H.S. Carslaw, J.C. Jaeger, Conduction of Heat in Solids, 2nd ed., Oxford University Press, London, 1959, pp. 282–296.
[9] S.H. Cho, J.E. Sunderland, Heat-conduction problems with melting or freezing, J. Heat Transfer 91 (1969) 421–426.
[10] N. Shamsundar, E.M. Sparrow, Analysis of multidimensional conduction phase change via the enthalpy model, J. Heat Transfer 97 (1975) 333–340.
[11] M. Lacroix, V.R. Voller, Finite difference solutions of solidification phase change problems: transformed versus fixed grids, Numer. Heat Transfer, Part B 17 (1990) 25–41.
[12] A.A. Rostami, R. Greif, R.E. Russo, Modified enthalpy method applied to rapid melting and solidification, Int. J. Heat Mass Transfer 35 (9) (1992) 2161–2172.
[13] J.M. Savino, R. Siegel, An analytical solution for solidification of a moving warm liquid onto an isothermal cold wall, Int. J. Heat Mass Transfer 12 (1969) 803–809.
[14] C.J. Flecher, Computational Techniques for Fluid Dynamics, vol. 1, 2nd ed., Springer, Berlin, 1991, p. 304.
[15] S.C. Sprott, Numerical Recipes, Cambridge University Press, Cambridge, 1991, pp. 254–259.